International Journal of Solids and Structures 51 (2014) 2979–2989

Contents lists available at ScienceDirect

International Journal of Solids and Structures

journal homepage: www.elsevier.com/locate/ijsolstr

A general closed-form solution for the overall response of piezoelectric composites with periodic and random particulate microstructures

Stephen A. Spinelli, Oscar Lopez-Pamies *

Department of Civil and Environmental Engineering, University of Illinois, Urbana–Champaign, IL 61801, USA

ARTICLE INFO

Article history:
Received 14 September 2013
Received in revised form 13 March 2014
Available online 20 April 2014

Keywords:
Electroactive materials
Microstructures
Iterated homogenization
Exact solutions

ABSTRACT

In this paper, we make use of a new iterative homogenization technique in finite electroelastostatics (Lopez-Pamies, 2014) to derive a closed-form solution for the overall response of two-phase piezoelectric composites with particulate microstructures. The calculations amount to solving a system of Riccati differential equations for the effective elastic, dielectric, and piezoelectric tensors of the composites, where the volume fraction of the inclusions plays the role of independent variable. The solution is valid for any choice of piezoelectric behaviors for the underlying matrix and inclusions, and any choice of the one- and two-point correlation functions describing the microstructure. In addition to discussing the key theoretical and practical features of the solution, its descriptive and predictive capabilities are illustrated via comparisons with a broad range of experimental data and full-field simulations (available from the literature) for composites with periodic and random distributions of inclusions of various shapes.

1. Introduction

This paper is concerned with generating an *exact closed-form* solution for the overall or macroscopic response of two-phase piezoelectric composites with particulate microstructures. At a microscopic level, a piezoelectric composite is taken to consist of a statistically uniform distribution of inclusions bonded perfectly to a continuous matrix phase. The domain occupied by the entire composite in its undeformed ground state is denoted by Ω. We assume that the characteristic length scales of the underlying inclusions are much smaller than the size of Ω and, for convenience, choose units of length so that Ω has unit volume. The constitutive behaviors of the matrix ($r = 1$) and the inclusions ($r = 2$) are characterized by "total" free energies $W^{(r)}$ that are functions of the deformation gradient tensor $\mathbf{F}$ and the Lagrangian electric field $\mathbf{E}$ so that at each material point $\mathbf{X} \in \Omega$ the first Piola–Kirchhoff stress tensor $\mathbf{S}$ and the Lagrangian electric displacement field $\mathbf{D}$ are given by (Dorfmann and Ogden, 2005; see also Suo et al., 2008)

$$\mathbf{S} = \frac{\partial W}{\partial \mathbf{F}}(\mathbf{X}, \mathbf{F}, \mathbf{E}) \quad \text{and} \quad \mathbf{D} = -\frac{\partial W}{\partial \mathbf{E}}(\mathbf{X}, \mathbf{F}, \mathbf{E}) \tag{1}$$

with

$$W(\mathbf{X}, \mathbf{F}, \mathbf{E}) = [1 - \theta^{(2)}(\mathbf{X})]W^{(1)}(\mathbf{F}, \mathbf{E}) + \theta^{(2)}(\mathbf{X})W^{(2)}(\mathbf{F}, \mathbf{E}), \tag{2}$$

where $\theta^{(2)}(\mathbf{X})$ stands for the indicator function of the regions occupied by the inclusions: $\theta^{(2)}(\mathbf{X}) = \mathbf{1}$ if $\mathbf{X}$ is inside an inclusion and $\theta^{(2)}(\mathbf{X}) = \mathbf{0}$ otherwise.

For periodic microstructures, the indicator function $\theta^{(2)}$ in (2) is completely known once a unit cell and the lattice over which it is repeated are specified. For random microstructures, on the other hand, $\theta^{(2)}$ is only known partially in a probabilistic sense. In either case, at any rate, we shall require but partial knowledge of $\theta^{(2)}$ in terms of the one- and two-point correlation functions. In view of the assumed statistical uniformity of the microstructure, these functions are insensitive to translations and thus given by (see, e.g., Chapter 15 in Milton (2002) and references therein)

$$p^{(2)} = \int_\Omega \theta^{(2)}(\mathbf{X})\,d\mathbf{X} \quad \text{and} \quad p^{(22)}(\mathbf{Z}) = \int_\Omega \theta^{(2)}(\mathbf{Z}+\mathbf{X})\theta^{(2)}(\mathbf{X})\,d\mathbf{X}. \tag{3}$$

Geometrically, the one-point correlation function $p^{(2)}$ represents the probability that a point lands in an inclusion when it is dropped randomly in Ω. In other words, $p^{(2)}$ is nothing more than the volume fraction of inclusions in the undeformed configuration; henceforth, we shall utilize the standard notation $p^{(2)} = c$. The two-point correlation function $p^{(22)}$ represents the probability that the ends of a rod of length and orientation described by the vector $\mathbf{Z}$ land within (the same or two different) inclusions when dropped randomly in Ω. Accordingly, $p^{(22)}$ contains finer information about the size, shape, and spatial distribution of the inclusions in the undeformed configuration.

* Corresponding author. Tel.: +1 (217) 244 1242.
E-mail addresses: sspinel2@illinois.edu (S.A. Spinelli), pamies@illinois.edu (O. Lopez-Pamies).

http://dx.doi.org/10.1016/j.ijsolstr.2014.04.009
0020-7683/

Granted the statistical uniformity of the microstructure and the separation between microscopic and macroscopic length scales, the overall constitutive response for the composite is defined as the relation between the volume averages of the first Piola–Kirchhoff stress $\bar{\mathbf{S}} \doteq \int_\Omega \mathbf{S}(\mathbf{X})\mathrm{d}\mathbf{X}$ and electric field $\bar{\mathbf{E}} \doteq \int_\Omega \mathbf{E}(\mathbf{X})\mathrm{d}\mathbf{X}$ and the volume averages of the deformation gradient $\bar{\mathbf{F}} \doteq \int_\Omega \mathbf{F}(\mathbf{X})\mathrm{d}\mathbf{X}$ and electric displacement $\bar{\mathbf{D}} \doteq \int_\Omega \mathbf{D}(\mathbf{X})\mathrm{d}\mathbf{X}$ over the undeformed configuration Ω when the composite is subjected to affine boundary conditions. This relation can be compactly written as (Lopez-Pamies, 2014)

$$\bar{\mathbf{S}} = \frac{\partial \bar{W}}{\partial \bar{\mathbf{F}}}(\bar{\mathbf{F}}, \bar{\mathbf{E}}, c) \quad \text{and} \quad \bar{\mathbf{D}} = -\frac{\partial \bar{W}}{\partial \bar{\mathbf{E}}}(\bar{\mathbf{F}}, \bar{\mathbf{E}}, c), \tag{4}$$

where the scalar-valued function

$$\bar{W}(\bar{\mathbf{F}}, \bar{\mathbf{E}}, c) = \min_{\mathbf{F}\in\mathcal{K}} \max_{\mathbf{E}\in\mathcal{E}} \int_\Omega W(\mathbf{X}, \mathbf{F}, \mathbf{E})\mathrm{d}\mathbf{X}, \tag{5}$$

referred to as the effective free energy function, corresponds physically to the total electroelastic free energy (per unit undeformed volume) of the composite. In these last expressions, the volume fraction of inclusions c has been included as an explicit argument in the effective energy $\bar{W}$ for later convenience and $\mathcal{K}$, $\mathcal{E}$ denote sufficiently large sets of admissible deformation gradients $\mathbf{F}$ and curl-free electric fields $\mathbf{E}$ with prescribed volume averages $\bar{\mathbf{F}}$ and $\bar{\mathbf{E}}$.

1.1. Linear piezoelectric behavior

The focus of this work is on the classical limit of *small macroscopic deformations* ($\bar{\mathbf{F}} \to \mathbf{I}$), when locally the composite is presumed to exhibit *linear piezoelectric behavior* characterized by a free energy function (2) of the asymptotic quadratic form

$$W(\mathbf{X}, \mathbf{F}, \mathbf{E}) = \frac{1}{2} H_{ij} L_{ijkl}(\mathbf{X}) H_{kl} - \frac{1}{2} E_i \epsilon_{ij}(\mathbf{X}) E_j - E_k e_{kij}(\mathbf{X}) H_{ij} \tag{6}$$

to leading order. Here, the notation $\mathbf{H} = \mathbf{F} - \mathbf{I}$ has been introduced for convenience, $\mathbf{L}(\mathbf{X}) = [1 - \theta^{(2)}(\mathbf{X})]\mathbf{L}^{(1)} + \theta^{(2)}(\mathbf{X})\mathbf{L}^{(2)}$ stands for the modulus tensor of elasticity measured at constant electric field ("short circuit"), $\boldsymbol{\epsilon}(\mathbf{X}) = [1 - \theta^{(2)}(\mathbf{X})]\boldsymbol{\epsilon}^{(1)} + \theta^{(2)}(\mathbf{X})\boldsymbol{\epsilon}^{(2)}$ denotes the dielectric tensor measured at constant deformation ("clamped"), and $\mathbf{e}(\mathbf{X}) = [1 - \theta^{(2)}(\mathbf{X})]\mathbf{e}^{(1)} + \theta^{(2)}(\mathbf{X})\mathbf{e}^{(2)}$ is the piezoelectric tensor[1]; these tensors exhibit the symmetries $L_{ijkl} = L_{klij} = L_{jikl} = L_{ijlk}$, $\epsilon_{ij} = \epsilon_{ji}$, $e_{kij} = e_{kji}$. The corresponding relations for the local stress and electric displacement (1) read as

$$S_{ij} = \frac{\partial W}{\partial F_{ij}}(\mathbf{X}, \mathbf{F}, \mathbf{E}) = L_{ijkl}(\mathbf{X}) H_{kl} - e_{kij}(\mathbf{X}) E_k \tag{7}$$

and

$$D_i = -\frac{\partial W}{\partial E_i}(\mathbf{X}, \mathbf{F}, \mathbf{E}) = \epsilon_{ij}(\mathbf{X}) E_j + e_{ipq}(\mathbf{X}) H_{pq}. \tag{8}$$

Owing to the quadratic form of the local free energy function (6), the resulting effective free energy function (5) in this case is quadratic in the macroscopic deformation gradient $\bar{\mathbf{F}}$ and electric field $\bar{\mathbf{E}}$:

$$\bar{W}(\bar{\mathbf{F}}, \bar{\mathbf{E}}, c) = \frac{1}{2} \bar{H}_{ij} \tilde{L}_{ijkl}(c) \bar{H}_{kl} - \frac{1}{2} \bar{E}_i \tilde{\epsilon}_{ij}(c) \bar{E}_j - \bar{E}_k \tilde{e}_{kij}(c) \bar{H}_{ij} \tag{9}$$

to leading order. Here, similar to the notation employed in (6), $\bar{\mathbf{H}} = \bar{\mathbf{F}} - \mathbf{I}$, while $\tilde{\mathbf{L}}$, $\tilde{\boldsymbol{\epsilon}}$, $\tilde{\mathbf{e}}$ stand for the effective "short-circuit" modulus of elasticity, the effective "clamped" dielectric tensor, and the effective piezoelectric tensor of the composite; they are such that $\tilde{L}_{ijkl} = \tilde{L}_{klij} = \tilde{L}_{jikl} = \tilde{L}_{ijlk}$, $\tilde{\epsilon}_{ij} = \tilde{\epsilon}_{ji}$, $\tilde{e}_{kij} = \tilde{e}_{kji}$. The corresponding macroscopic stress and electric displacement (4) take then the simple linear piezoelectric form

$$\bar{S}_{ij} = \frac{\partial \bar{W}}{\partial \bar{F}_{ij}}(\bar{\mathbf{F}}, \bar{\mathbf{E}}) = \tilde{L}_{ijkl}(c) \bar{H}_{kl} - \tilde{e}_{kij}(c) \bar{E}_k \tag{10}$$

and

$$\bar{D}_i = -\frac{\partial \bar{W}}{\partial \bar{E}_i}(\bar{\mathbf{F}}, \bar{\mathbf{E}}) = \tilde{\epsilon}_{ij}(c) \bar{E}_j + \tilde{e}_{ipq}(c) \bar{H}_{pq}. \tag{11}$$

The objective of this work reduces hence to generating a solution for the effective tensors $\tilde{\mathbf{L}}$, $\tilde{\boldsymbol{\epsilon}}$, $\tilde{\mathbf{e}}$ in (9) directly in terms of the properties of the matrix $\mathbf{L}^{(1)}$, $\boldsymbol{\epsilon}^{(1)}$, $\mathbf{e}^{(1)}$, the properties of the inclusions $\mathbf{L}^{(2)}$, $\boldsymbol{\epsilon}^{(2)}$, $\mathbf{e}^{(2)}$, and the microstructure — the size, the shape, and the spatial distribution of the inclusions — as characterized by the indicator function $\theta^{(2)}$. To this end, we will make use of a new theory for elastic dielectric composites recently introduced by Lopez-Pamies (2014). For convenience and clarity, the general form of this theory is presented in the next section. Its application to the piezoelectric composites of interest here and the closed-form solution for the effective tensors $\tilde{\mathbf{L}}$, $\tilde{\boldsymbol{\epsilon}}$, $\tilde{\mathbf{e}}$ that it generates — Eq. (36) — are presented in Section 3. That section also includes a discussion of the key theoretical and practical features of this closed-form solution, as well as its specialization to various cases of practical relevance. Finally, Section 4 confronts the solution to a host of experimental data and full-field simulations available in the literature.

2. The theory of Lopez-Pamies (2014) for elastic dielectric composites

By means of a combination of iterative techniques, Lopez-Pamies (2014) has recently generated an exact solution for the variational problem (5) for two-phase elastic dielectric composites with a specific, yet fairly general, class of particulate microstructures. In the present notation, his result for the effective free energy function $\bar{W} = \bar{W}(\bar{\mathbf{F}}, \bar{\mathbf{E}}, c)$ is given implicitly by the first-order partial differential equation (pde)

$$\mathrm{c}\frac{\partial \bar{W}}{\partial \mathrm{c}} - \bar{W} - \int_{|\boldsymbol{\xi}|=1} \max_{\boldsymbol{\alpha}} \min_{\beta} \Big[\boldsymbol{\alpha} \cdot \frac{\partial \bar{W}}{\partial \bar{\mathbf{F}}} \boldsymbol{\xi} + \beta \frac{\partial \bar{W}}{\partial \bar{\mathbf{E}}} \cdot \boldsymbol{\xi} - W^{(1)}(\bar{\mathbf{F}} + \boldsymbol{\alpha} \otimes \boldsymbol{\xi}, \bar{\mathbf{E}} + \beta\boldsymbol{\xi}) \Big] \nu(\boldsymbol{\xi})\mathrm{d}\boldsymbol{\xi} = 0 \tag{12}$$

subject to the initial condition

$$\bar{W}(\bar{\mathbf{F}}, \bar{\mathbf{E}}, 1) = W^{(2)}(\bar{\mathbf{F}}, \bar{\mathbf{E}}), \tag{13}$$

where the integration of the pde (12) is to be carried out from $\mathrm{c} = 1$ to the desired final value of volume fraction of inclusions $\mathrm{c} = c$ and the weighting function $\nu(\boldsymbol{\xi})$ in (12) is given in terms of the two-point correlation function $(3)_2$ as follows:

- *Periodic microstructures*. For the case of periodic distributions of inclusions, the function $\nu(\boldsymbol{\xi})$ is given by

$$\nu(\boldsymbol{\xi}) = \sum_{\mathbf{k}\in\mathcal{R}^*-\{\mathbf{0}\}} \frac{\hat{p}^{(22)}(\mathbf{k})}{(1-c)c} \delta\Big(\boldsymbol{\xi} - \frac{\mathbf{k}}{|\mathbf{k}|}\Big) \quad \text{with}$$
$$\hat{p}^{(22)}(\mathbf{k}) = \frac{1}{|Q|} \int_Q p^{(22)}(\mathbf{X}) e^{-\mathrm{i}\mathbf{X}\cdot\mathbf{k}} \mathrm{d}\mathbf{X}. \tag{14}$$

Here, $\delta(\boldsymbol{\xi} - \mathbf{k}/|\mathbf{k}|)$ denotes the Dirac delta function and $\hat{p}^{(22)}(\mathbf{k})$ stands for the Fourier transform of the two-point correlation function $p^{(22)}(\mathbf{X})$, while Q denotes the repeating unit cell chosen to describe the microstructure and

$$\mathcal{R}^* = \{\mathbf{k} : \mathbf{k} = n_1\mathbf{B}_1 + n_2\mathbf{B}_2 + n_3\mathbf{B}_3, \quad n_i \in \mathbb{Z}\} \tag{15}$$

[1] The alternative classical formulations can be found, for instance, in Standards on Piezoelectric Crystals (1949), where the moduli L_{ijkl}, e_{ijk}, and ϵ_{ij} appear as C^E_{ijkl}, e_{ijk}, and ϵ^S_{ij}, respectively.

with

$$\mathbf{B}_1 = 2\pi\frac{\mathbf{A}_2\wedge\mathbf{A}_3}{\mathbf{A}_1\cdot(\mathbf{A}_2\wedge\mathbf{A}_3)},\quad \mathbf{B}_2 = 2\pi\frac{\mathbf{A}_3\wedge\mathbf{A}_1}{\mathbf{A}_1\cdot(\mathbf{A}_2\wedge\mathbf{A}_3)},$$
$$\mathbf{B}_3 = 2\pi\frac{\mathbf{A}_1\wedge\mathbf{A}_2}{\mathbf{A}_1\cdot(\mathbf{A}_2\wedge\mathbf{A}_3)} \tag{16}$$

stands for the reciprocal lattice in Fourier space of the periodic lattice in real space

$$\mathcal{R} = \{\mathbf{Y} : \mathbf{Y} = n_1\mathbf{A}_1 + n_2\mathbf{A}_2 + n_3\mathbf{A}_3,\quad n_i\in\mathbb{Z}\} \tag{17}$$

over which the unit cell Q is repeated (see, e.g., Kittel, 2005). Upon invoking the identity $\hat{p}^{(22)}(\mathbf{k}) = |\hat{\theta}^{(2)}(\mathbf{k})|^2$ with $\hat{\theta}^{(2)}(\mathbf{k}) = |Q|^{-1}\int_Q \theta^{(2)}(\mathbf{X})e^{-i\mathbf{k}\cdot\mathbf{X}}\,d\mathbf{X}$, it is noteworthy to recognize that the pde (12) adopts the more explicit form

$$c\frac{\partial\bar{W}}{\partial c} - \bar{W} - \sum_{\substack{\mathbf{k}\in\mathcal{R}^*-\{\mathbf{0}\}\\ \xi=\mathbf{k}/|\mathbf{k}|}}\left\{\max_{\boldsymbol{\alpha}}\min_{\beta}\left[\boldsymbol{\alpha}\cdot\frac{\partial\bar{W}}{\partial\bar{\mathbf{F}}}\xi + \beta\frac{\partial\bar{W}}{\partial\bar{\mathbf{E}}}\cdot\xi - W^{(1)}\left(\bar{\mathbf{F}}+\boldsymbol{\alpha}\otimes\xi,\bar{\mathbf{E}}+\beta\xi\right)\right]\frac{|\hat{\theta}^{(2)}(\mathbf{k})|^2}{(1-c)c}\right\} = 0. \tag{18}$$

- *Random microstructures*. For the case of random distributions of inclusions, the function $v(\xi)$ is given by

$$v(\xi) = -\frac{1}{8\pi^2}\int_\Omega \frac{p^{(22)}(\mathbf{X}) - c^2}{(1-c)c}\delta''(\xi\cdot\mathbf{X})\,d\mathbf{X}, \tag{19}$$

where δ'' denotes the second derivative of the Dirac delta function with respect to its argument. Direct use of relation (19) allows to rewrite the pde (12) more explicitly as

$$c\frac{\partial\bar{W}}{\partial c} - \bar{W} + \frac{1}{8\pi^2}\int_{|\xi|=1}\int_\Omega \max_{\boldsymbol{\alpha}}\min_{\beta}\left[\boldsymbol{\alpha}\cdot\frac{\partial\bar{W}}{\partial\bar{\mathbf{F}}}\xi + \beta\frac{\partial\bar{W}}{\partial\bar{\mathbf{E}}}\cdot\xi - W^{(1)}\left(\bar{\mathbf{F}}+\boldsymbol{\alpha}\otimes\xi,\bar{\mathbf{E}}+\beta\xi\right)\right]\frac{p^{(22)}(\mathbf{X}) - c^2}{(1-c)c}\delta''(\xi\cdot\mathbf{X})d\mathbf{X}d\xi = 0. \tag{20}$$

The interested reader is referred to Lopez-Pamies (2014) for the derivation and thorough discussion of the above result. At this stage, nevertheless, it is appropriate to remark that the result (12) and (13) is exact for a specific class of two-phase particulate microstructures and hence it is realizable. What is more, in view of its applicability to arbitrary free energy functions $W^{(1)}$ and $W^{(2)}$ and arbitrary one-point $p^{(2)}$ and two-point $p^{(22)}$ correlation functions, the result (12) and (13) can be utilized more generally as a constitutive theory for two-phase elastic dielectrics with *any* particulate microstructure: for a given matrix constitutive behavior $W^{(1)}$, given inclusion constitutive behavior $W^{(2)}$, and given one- and two-point correlations $p^{(2)}$ and $p^{(22)}$, the result (12) and (13) provides a constitutive model for the macroscopic response of the elastic dielectric composite of interest.

3. A closed-form solution for piezoelectric composites

When the constitutive behavior of the matrix and inclusions is characterized by the piezoelectric free energy function (6), it is a simple matter to show that the solution to the pde (12) with initial condition (13) is indeed of the quadratic functional form (9). In turn, a simple calculation suffices to deduce that the conditions defining the maximizing vector $\boldsymbol{\alpha}$ and minimizing scalar β in (12) specialize to the following system of algebraic equations:

$$\left[\Delta\tilde{L}_{ijkl}\bar{H}_{kl} - \Delta\tilde{e}_{kij}\bar{E}_k - L^{(1)}_{ijkl}\alpha_k\xi_l + e^{(1)}_{mij}\beta\xi_m\right]\xi_j = 0 \tag{21}$$

and

$$\left[\Delta\tilde{\epsilon}_{ij}\bar{E}_j + \Delta\tilde{e}_{ikl}\bar{H}_{kl} - \epsilon^{(1)}_{ij}\beta\xi_j - e^{(1)}_{ikl}\alpha_k\xi_l\right]\xi_i = 0, \tag{22}$$

where the notation $\Delta\tilde{\mathbf{L}} = \tilde{\mathbf{L}} - \mathbf{L}^{(1)}$, $\Delta\tilde{\boldsymbol{\epsilon}} = \tilde{\boldsymbol{\epsilon}} - \boldsymbol{\epsilon}^{(1)}$, $\Delta\tilde{\mathbf{e}} = \tilde{\mathbf{e}} - \mathbf{e}^{(1)}$ has been introduced for convenience. Eqs. (21) and (22) can be solved explicitly to render

$$\alpha_k\xi_l = \left[\Gamma^L_{klpq}(\xi)\Delta\tilde{L}_{pqrs} + \Gamma^e_{kln}(\xi)\Delta\tilde{e}_{nrs}\right]\bar{H}_{rs} + \left[\Gamma^e_{klr}(\xi)\Delta\tilde{\epsilon}_{rs} - \Gamma^L_{klpq}(\xi)\Delta\tilde{e}_{spq}\right]\bar{E}_s \tag{23}$$

and

$$\beta\xi_j = \left[-\Gamma^e_{pqj}(\xi)\Delta\tilde{L}_{pqrs} + \Gamma^\epsilon_{jn}(\xi)\Delta\tilde{e}_{nrs}\right]\bar{H}_{rs} + \left[\Gamma^\epsilon_{jn}(\xi)\Delta\tilde{\epsilon}_{ns} + \Gamma^e_{pqj}(\xi)\Delta\tilde{e}_{spq}\right]\bar{E}_s, \tag{24}$$

where

$$\Gamma^L_{klpq}(\xi) = K^{-1}_{kp}(\xi)\xi_q\xi_l,$$
$$\Gamma^\epsilon_{jn}(\xi) = \frac{1}{\epsilon^{(1)}_{ab}\xi_a\xi_b}\xi_j\xi_n - \frac{1}{\left(\epsilon^{(1)}_{ab}\xi_a\xi_b\right)^2}K^{-1}_{kp}(\xi)e^{(1)}_{mpq}e^{(1)}_{ikl}\xi_q\xi_l\xi_m\xi_n\xi_i\xi_j,$$
$$\Gamma^e_{kln}(\xi) = \frac{1}{\epsilon^{(1)}_{ab}\xi_a\xi_b}K^{-1}_{kp}(\xi)e^{(1)}_{mpq}\xi_q\xi_l\xi_m\xi_n \tag{25}$$

with

$$K_{ik}(\xi) = L^{(1)}_{ijkl}\xi_j\xi_l + \frac{1}{\epsilon^{(1)}_{ab}\xi_a\xi_b}e^{(1)}_{mij}e^{(1)}_{qkr}\xi_m\xi_j\xi_q\xi_r. \tag{26}$$

Note that the second-order tensor (26) is nothing more than the generalized acoustic tensor associated with the piezoelectric matrix material $r = 1$. Note also that the tensors $\boldsymbol{\Gamma}^L$, $\boldsymbol{\Gamma}^\epsilon$, $\boldsymbol{\Gamma}^e$ are homogeneous functions of degree zero in ξ with symmetries $\Gamma^L_{klpq} = \Gamma^L_{pqkl}$, $\Gamma^\epsilon_{jn} = \Gamma^\epsilon_{nj}$, $\Gamma^e_{kln} = \Gamma^e_{knl}$.

By making direct use of expressions (6), (9), (23), (24) and subsequently grouping the terms of order $||\bar{\mathbf{H}}||^2$, $||\bar{\mathbf{E}}||^2$, $||\bar{\mathbf{H}}||||\bar{\mathbf{E}}||$, the pde (12) with initial condition (13) for the effective free energy function $\bar{W}$ can be shown to reduce, rather interestingly, to the following system of Riccati ordinary differential equations (odes):

$$c\frac{\partial\tilde{L}_{mnrs}}{\partial c} - \Delta\tilde{L}_{mnrs} - \Delta\tilde{L}_{mnkl}P^L_{klpq}\Delta\tilde{L}_{pqrs} + \Delta\tilde{e}_{kmn}P^\epsilon_{kl}\Delta\tilde{e}_{lrs} - \Delta\tilde{L}_{mnij}P^e_{ijk}\Delta\tilde{e}_{krs} - \Delta\tilde{L}_{rsij}P^e_{ijk}\Delta\tilde{e}_{kmn} = 0, \tag{27}$$

$$c\frac{\partial\tilde{\epsilon}_{pq}}{\partial c} - \Delta\tilde{\epsilon}_{pq} - \Delta\tilde{\epsilon}_{pk}P^\epsilon_{kl}\Delta\tilde{\epsilon}_{lq} + \Delta\tilde{e}_{pkl}P^L_{klmn}\Delta\tilde{e}_{qmn} - \Delta\tilde{\epsilon}_{pk}P^e_{ijk}\Delta\tilde{e}_{qij} - \Delta\tilde{\epsilon}_{qk}P^e_{ijk}\Delta\tilde{e}_{pij} = 0, \tag{28}$$

$$c\frac{\partial\tilde{e}_{qmn}}{\partial c} - \Delta\tilde{e}_{qmn} - \Delta\tilde{e}_{kmn}P^e_{ijk}\Delta\tilde{e}_{qij} + \Delta\tilde{L}_{mnij}P^e_{ijk}\Delta\tilde{\epsilon}_{kq} - \Delta\tilde{L}_{mnij}P^L_{ijkl}\Delta\tilde{e}_{qkl} - \Delta\tilde{\epsilon}_{qk}P^\epsilon_{kl}\Delta\tilde{e}_{lmn} = 0 \tag{29}$$

for the effective tensors $\tilde{\mathbf{L}} = \tilde{\mathbf{L}}(c)$, $\tilde{\boldsymbol{\epsilon}} = \tilde{\boldsymbol{\epsilon}}(c)$, $\tilde{\mathbf{e}} = \tilde{\mathbf{e}}(c)$, subject to the initial conditions

$$\tilde{\mathbf{L}}(1) = \mathbf{L}^{(2)},\quad \tilde{\boldsymbol{\epsilon}}(1) = \boldsymbol{\epsilon}^{(2)},\quad \tilde{\mathbf{e}}(1) = \mathbf{e}^{(2)}. \tag{30}$$

In these last expressions, we have made use of the notation

$$P^L_{klpq} = \int_{|\xi|=1}\frac{1}{4}\left[\Gamma^L_{klpq}(\xi) + \Gamma^L_{lkpq}(\xi) + \Gamma^L_{klqp}(\xi) + \Gamma^L_{lkqp}(\xi)\right]v(\xi)d\xi,$$
$$P^\epsilon_{kl} = \int_{|\xi|=1}\Gamma^\epsilon_{kl}(\xi)v(\xi)d\xi,$$
$$P^e_{ijk} = \int_{|\xi|=1}\frac{1}{2}\left[\Gamma^e_{ijk}(\xi) + \Gamma^e_{jik}(\xi)\right]v(\xi)d\xi, \tag{31}$$

where it is recalled that the weighting function $v(\xi)$ in these orientational averages is given by expression $(14)_1$ for periodic microstructures and by (19) for random ones in terms of the two-point correlation function.

In spite of the fact that the system of Riccati odes (27)–(29) is coupled and nonlinear, it can be solved explicitly by rewriting the equations in terms of an augmented matrix representation of the effective tensors $\tilde{\mathbf{L}}$, $\tilde{\boldsymbol{\epsilon}}$, $\tilde{\mathbf{e}}$, instead of directly in terms of the tensors $\tilde{\mathbf{L}}$, $\tilde{\boldsymbol{\epsilon}}$, $\tilde{\mathbf{e}}$. Indeed, by introducing the 9×9 symmetric matrices

$$\mathsf{L}^{(r)}=\begin{bmatrix} L^{(r)}_{1111} & L^{(r)}_{1122} & L^{(r)}_{1133} & L^{(r)}_{1112} & L^{(r)}_{1113} & L^{(r)}_{1123} & -e^{(r)}_{111} & -e^{(r)}_{211} & -e^{(r)}_{311}\\ L^{(r)}_{1122} & L^{(r)}_{2222} & L^{(r)}_{2233} & L^{(r)}_{2212} & L^{(r)}_{2213} & L^{(r)}_{2223} & -e^{(r)}_{122} & -e^{(r)}_{222} & -e^{(r)}_{322}\\ L^{(r)}_{1133} & L^{(r)}_{2233} & L^{(r)}_{3333} & L^{(r)}_{3312} & L^{(r)}_{3313} & L^{(r)}_{3323} & -e^{(r)}_{133} & -e^{(r)}_{233} & -e^{(r)}_{333}\\ L^{(r)}_{1112} & L^{(r)}_{2212} & L^{(r)}_{3312} & L^{(r)}_{1212} & L^{(r)}_{1213} & L^{(r)}_{1223} & -e^{(r)}_{112} & -e^{(r)}_{212} & -e^{(r)}_{312}\\ L^{(r)}_{1113} & L^{(r)}_{2213} & L^{(r)}_{3313} & L^{(r)}_{1213} & L^{(r)}_{1313} & L^{(r)}_{1323} & -e^{(r)}_{113} & -e^{(r)}_{213} & -e^{(r)}_{313}\\ L^{(r)}_{1123} & L^{(r)}_{2223} & L^{(r)}_{3323} & L^{(r)}_{1223} & L^{(r)}_{1323} & L^{(r)}_{2323} & -e^{(r)}_{123} & -e^{(r)}_{223} & -e^{(r)}_{323}\\ -e^{(r)}_{111} & -e^{(r)}_{122} & -e^{(r)}_{133} & -e^{(r)}_{112} & -e^{(r)}_{113} & -e^{(r)}_{123} & \epsilon^{(r)}_{11} & \epsilon^{(r)}_{12} & \epsilon^{(r)}_{13}\\ -e^{(r)}_{211} & -e^{(r)}_{222} & -e^{(r)}_{233} & -e^{(r)}_{212} & -e^{(r)}_{213} & -e^{(r)}_{223} & \epsilon^{(r)}_{12} & \epsilon^{(r)}_{22} & \epsilon^{(r)}_{23}\\ -e^{(r)}_{311} & -e^{(r)}_{322} & -e^{(r)}_{333} & -e^{(r)}_{312} & -e^{(r)}_{313} & -e^{(r)}_{323} & \epsilon^{(r)}_{13} & \epsilon^{(r)}_{23} & \epsilon^{(r)}_{33}\end{bmatrix},\quad r=1,2, \tag{32}$$

$$\mathsf{P}=\begin{bmatrix} P^{L}_{1111} & P^{L}_{1122} & P^{L}_{1133} & 2P^{L}_{1112} & 2P^{L}_{1113} & 2P^{L}_{1123} & -P^{e}_{111} & -P^{e}_{112} & -P^{e}_{113}\\ P^{L}_{1122} & P^{L}_{2222} & P^{L}_{2233} & 2P^{L}_{2212} & 2P^{L}_{2213} & 2P^{L}_{2223} & -P^{e}_{221} & -P^{e}_{222} & -P^{e}_{223}\\ P^{L}_{1133} & P^{L}_{2233} & P^{L}_{3333} & 2P^{L}_{3312} & 2P^{L}_{3313} & 2P^{L}_{3323} & -P^{e}_{331} & -P^{e}_{332} & -P^{e}_{333}\\ 2P^{L}_{1112} & 2P^{L}_{2212} & 2P^{L}_{3312} & 4P^{L}_{1212} & 4P^{L}_{1213} & 4P^{L}_{1223} & -2P^{e}_{121} & -2P^{e}_{122} & -2P^{e}_{123}\\ 2P^{L}_{1113} & 2P^{L}_{2213} & 2P^{L}_{3313} & 4P^{L}_{1213} & 4P^{L}_{1313} & 4P^{L}_{1323} & -2P^{e}_{131} & -2P^{e}_{132} & -2P^{e}_{133}\\ 2P^{L}_{1123} & 2P^{L}_{2223} & 2P^{L}_{3323} & 4P^{L}_{1223} & 4P^{L}_{1323} & 4P^{L}_{2323} & -2P^{e}_{231} & -2P^{e}_{232} & -2P^{e}_{233}\\ -P^{e}_{111} & -P^{e}_{221} & -P^{e}_{331} & -2P^{e}_{121} & -2P^{e}_{131} & -2P^{e}_{231} & -P^{\epsilon}_{11} & -P^{\epsilon}_{12} & -P^{\epsilon}_{13}\\ -P^{e}_{112} & -P^{e}_{222} & -P^{e}_{332} & -2P^{e}_{122} & -2P^{e}_{132} & -2P^{e}_{232} & -P^{\epsilon}_{12} & -P^{\epsilon}_{22} & -P^{\epsilon}_{23}\\ -P^{e}_{113} & -P^{e}_{223} & -P^{e}_{333} & -2P^{e}_{123} & -2P^{e}_{133} & -2P^{e}_{233} & -P^{\epsilon}_{13} & -P^{\epsilon}_{23} & -P^{\epsilon}_{33}\end{bmatrix}, \tag{33}$$

and

$$\tilde{\mathsf{L}}=\begin{bmatrix} \tilde{L}_{1111} & \tilde{L}_{1122} & \tilde{L}_{1133} & \tilde{L}_{1112} & \tilde{L}_{1113} & \tilde{L}_{1123} & -\tilde{e}_{111} & -\tilde{e}_{211} & -\tilde{e}_{311}\\ \tilde{L}_{1122} & \tilde{L}_{2222} & \tilde{L}_{2233} & \tilde{L}_{2212} & \tilde{L}_{2213} & \tilde{L}_{2223} & -\tilde{e}_{122} & -\tilde{e}_{222} & -\tilde{e}_{322}\\ \tilde{L}_{1133} & \tilde{L}_{2233} & \tilde{L}_{3333} & \tilde{L}_{3312} & \tilde{L}_{3313} & \tilde{L}_{3323} & -\tilde{e}_{133} & -\tilde{e}_{233} & -\tilde{e}_{333}\\ \tilde{L}_{1112} & \tilde{L}_{2212} & \tilde{L}_{3312} & \tilde{L}_{1212} & \tilde{L}_{1213} & \tilde{L}_{1223} & -\tilde{e}_{112} & -\tilde{e}_{212} & -\tilde{e}_{312}\\ \tilde{L}_{1113} & \tilde{L}_{2213} & \tilde{L}_{3313} & \tilde{L}_{1213} & \tilde{L}_{1313} & \tilde{L}_{1323} & -\tilde{e}_{113} & -\tilde{e}_{213} & -\tilde{e}_{313}\\ \tilde{L}_{1123} & \tilde{L}_{2223} & \tilde{L}_{3323} & \tilde{L}_{1223} & \tilde{L}_{1323} & \tilde{L}_{2323} & -\tilde{e}_{123} & -\tilde{e}_{223} & -\tilde{e}_{323}\\ -\tilde{e}_{111} & -\tilde{e}_{122} & -\tilde{e}_{133} & -\tilde{e}_{112} & -\tilde{e}_{113} & -\tilde{e}_{123} & \tilde{\epsilon}_{11} & \tilde{\epsilon}_{12} & \tilde{\epsilon}_{13}\\ -\tilde{e}_{211} & -\tilde{e}_{222} & -\tilde{e}_{233} & -\tilde{e}_{212} & -\tilde{e}_{213} & -\tilde{e}_{223} & \tilde{\epsilon}_{12} & \tilde{\epsilon}_{22} & \tilde{\epsilon}_{23}\\ -\tilde{e}_{311} & -\tilde{e}_{322} & -\tilde{e}_{333} & -\tilde{e}_{312} & -\tilde{e}_{313} & -\tilde{e}_{323} & \tilde{\epsilon}_{13} & \tilde{\epsilon}_{23} & \tilde{\epsilon}_{33}\end{bmatrix}, \tag{34}$$

the system of Riccati odes (27)–(29) subject to the initial conditions (30) can be rewritten more compactly as the Riccati initial-value problem

$$c\frac{d\tilde{\mathsf{L}}}{dc}-\Delta\tilde{\mathsf{L}}-\Delta\tilde{\mathsf{L}}\mathsf{P}\Delta\tilde{\mathsf{L}}=0\quad\text{with}\quad\tilde{\mathsf{L}}(1)=\mathsf{L}^{(2)} \tag{35}$$

for the matrix $\tilde{\mathsf{L}}=\tilde{\mathsf{L}}(c)$, where use has been made of the notation $\Delta\tilde{\mathsf{L}}=\tilde{\mathsf{L}}-\mathsf{L}^{(1)}$. The solution to this initial-value problem is given by

$$\tilde{\mathsf{L}}=\mathsf{L}^{(1)}+c\left[(1-c)\mathsf{P}+\left(\mathsf{L}^{(2)}-\mathsf{L}^{(1)}\right)^{-1}\right]^{-1}. \tag{36}$$

The simple *exact closed-form* solution (36) constitutes the main result of this paper. It characterizes the overall response of two-phase piezoelectric composites with a large class of periodic and random particulate microstructures. The following theoretical and practical remarks are in order:

1. *Piezoelectric behaviors of the matrix and inclusions*. The solution (36) is valid for any choice of elastic moduli $\mathbf{L}^{(1)}$ and $\mathbf{L}^{(2)}$, dielectric tensors $\boldsymbol{\epsilon}^{(1)}$ and $\boldsymbol{\epsilon}^{(2)}$, and piezoelectric tensors $\mathbf{e}^{(1)}$ and $\mathbf{e}^{(2)}$ describing the piezoelectric behaviors of the underlying matrix and inclusions.
2. *Geometry and spatial distribution of the inclusions*. The solution (36) is also valid for any choice of the one- and two-point correlation functions $p^{(2)}=c$ and $p^{(22)}$ describing the microstructure. In practice, both of these quantities are generally measurable and often times readily known from the outset.
3. *Connections with the dilute result of* Deeg (1980) *for ellipsoidal inclusions and the Hashin–Shtrikman variational principle*. By construction, the underlying microstructure associated with the solution (36) corresponds to a distribution of disconnected inclusions that interact in such a manner that their deformation gradient and electric field — irrespectively of the value of the volume fraction of inclusions c — are *uniform* and the *same* in each inclusion (see Appendix B in Lopez-Pamies (2014)).
   An interesting implication of such a special type of intra-inclusion fields is that the exact solution (36) corresponds, in essence, to an extension of the classical result[2] of Deeg (1980) for a dilute distribution of ellipsoidal inclusions — wherein the electromechanical fields are uniform — to distributions of inclusions of more general shapes and finite volume fraction.
   A further implication of the uniformity of the intra-inclusion fields is that the solution (36) agrees identically with the variational approximation obtained from the Hashin–Shtrikman variational principle (Bisegna and Luciano, 1996; see also Olson and Avellaneda, 1992; Li and Dunn, 2001) when choosing the reference medium to coincide with the piezoelectric matrix material and the trial polarization field to be constant per phase (so that the fields within the inclusions are also constant). A corollary of this agreement is that the solution (36) coincides identically with one of the Hashin–Shtrikman bounds when the piezoelectric properties of the matrix and inclusions are well ordered.
4. *Computational tractability*. In spite of its generality and incorporation of fine microscopic information, the computation of the solution (36) is admittedly simple, as it only requires the evaluation of the microstructural tensors $\mathbf{P}^{L}$, $\mathbf{P}^{\epsilon}$, $\mathbf{P}^{e}$ defined in (31). The next subsection spells out the specializations of these tensors to several cases of practical relevance.

3.1. Some special cases

For demonstration purposes and later use in comparisons with experiments and full-field simulations, we spell out next the specializations of the microstructural tensors $\mathbf{P}^{L}$, $\mathbf{P}^{\epsilon}$, $\mathbf{P}^{e}$ — needed in the computation of the solution (36) — to three classes of microstructures with ellipsoidal and cuboidal inclusions (see Fig. 1). These shapes include as limiting cases spherical and cubic inclusions, cylindrical fibers with elliptical and rectangular cross sections, and layers. Such geometries have repeatedly proved of relevance in a variety of applications (see, e.g., Banno, 1987; Chan and Unsworth, 1989; Bast and Wersing, 1989).

3.1.1. A periodic distribution of ellipsoidal inclusions

We begin by considering a periodic distribution of ellipsoidal inclusions where the repeating unit cell comprises a rectangular prism of sides b_1, b_2, b_3 containing a single inclusion located at its center. As depicted in Fig. 1(a), the inclusion has semi-axes a_1, a_2, a_3 and its principal axes are coaxial with those of the unit cell which, for convenience, are chosen to coincide with the Cartesian laboratory axes $\mathbf{u}_1$, $\mathbf{u}_2$, $\mathbf{u}_3$. For this class of periodic microstructures, it is

[2] See also Dunn and Taya (1993).

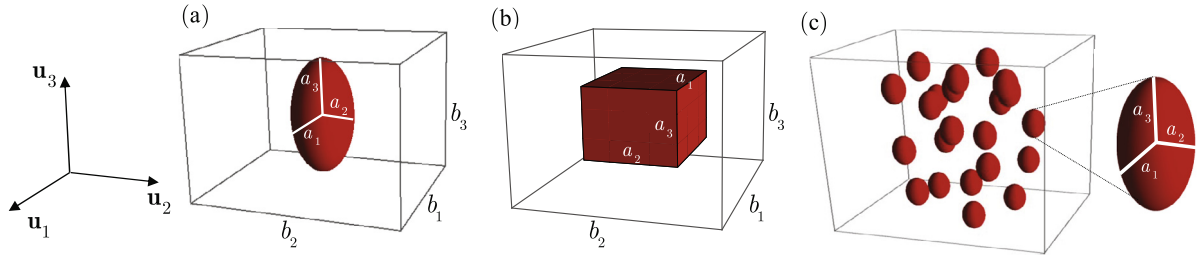

Fig. 1. Schematics of the three classes of particulate microstructures considered in Sections 3.1.1–3.1.3. Parts (a) and (b) show, respectively, rectangular prismatic unit cells, with sides $b_1,\ b_2,\ b_3$, describing *periodic* cuboidal distributions of ellipsoidal and cuboidal inclusions. Part (c) depicts a *random* microstructure comprised of aligned homothetic ellipsoidal inclusions whose centers are distributed with "ellipsoidal" symmetry.

not difficult to compute the Fourier transform $(14)_2$ of its two-point correlation function and reciprocal lattice (15) and (16) in order to deduce that the microstructural tensors (31) specialize to

$$P^L_{ijkl} = \frac{c}{1-c}\sum_{\substack{\mathrm{p}_1=-\infty\\ -\{\mathrm{p}_1=\mathrm{p}_2=\mathrm{p}_3=0\}}}^{\infty}\sum_{\mathrm{p}_2=-\infty}^{\infty}\sum_{\mathrm{p}_3=-\infty}^{\infty}\frac{1}{4}\left[\Gamma^L_{ijkl}(\boldsymbol{\xi})+\Gamma^L_{jikl}(\boldsymbol{\xi})+\Gamma^L_{ijlk}(\boldsymbol{\xi})+\Gamma^L_{jilk}(\boldsymbol{\xi})\right]g^2(\boldsymbol{\xi}),$$

$$P^\epsilon_{ij} = \frac{c}{1-c}\sum_{\substack{\mathrm{p}_1=-\infty\\ -\{\mathrm{p}_1=\mathrm{p}_2=\mathrm{p}_3=0\}}}^{\infty}\sum_{\mathrm{p}_2=-\infty}^{\infty}\sum_{\mathrm{p}_3=-\infty}^{\infty}\Gamma^\epsilon_{ij}(\boldsymbol{\xi})\,g^2(\boldsymbol{\xi}), \tag{37}$$

$$P^e_{ijk} = \frac{c}{1-c}\sum_{\substack{\mathrm{p}_1=-\infty\\ -\{\mathrm{p}_1=\mathrm{p}_2=\mathrm{p}_3=0\}}}^{\infty}\sum_{\mathrm{p}_2=-\infty}^{\infty}\sum_{\mathrm{p}_3=-\infty}^{\infty}\frac{1}{2}\left[\Gamma^e_{ijk}(\boldsymbol{\xi})+\Gamma^e_{jik}(\boldsymbol{\xi})\right]g^2(\boldsymbol{\xi}).$$

Here, it is recalled that the tensors $\boldsymbol{\Gamma}^L, \boldsymbol{\Gamma}^\epsilon, \boldsymbol{\Gamma}^e$ are given by expressions (25), $c = 4\pi a_1a_2a_3/3b_1b_2b_3$,

$$\boldsymbol{\xi} = \mathrm{p}_1\mathbf{u}_1 + \frac{b_1}{b_2}\mathrm{p}_2\mathbf{u}_2 + \frac{b_1}{b_3}\mathrm{p}_3\mathbf{u}_3 \tag{38}$$

in terms of the integers p_1, p_2, p_3, and the function $g(\xi)$ is given by

$$g(\xi) = \frac{3(\sin\eta-\eta\cos\eta)}{\eta^3} \quad \text{with} \quad \eta = 2\pi\sqrt{\frac{a_1^2}{b_1^2}\mathrm{p}_1^2+\frac{a_2^2}{b_2^2}\mathrm{p}_2^2+\frac{a_3^2}{b_3^2}\mathrm{p}_3^2}. \tag{39}$$

As pointed out above, expressions (37) contain several limiting cases worth placing on record. The case of a cuboidal distribution of *spherical inclusions* is trivially generated by setting $a_1 = a_2 = a_3 = a$ in (37). The case of a rectangular distribution of aligned *cylindrical fibers* with elliptical cross section is generated by setting one of the semi-axes of the inclusion and the corresponding side of the unit cell to be of infinite length. By setting $a_m,\ b_m = \infty\,(m, n,\ s = 1, 2, 3)$, for instance, the general expressions (37) reduce to

$$P^L_{ijkl} = \frac{c}{1-c}\sum_{\substack{\mathrm{p}_n=-\infty\\ -\{\mathrm{p}_n=\mathrm{p}_s=0\}}}^{\infty}\sum_{\mathrm{p}_s=-\infty}^{\infty}\frac{1}{4}\left[\Gamma^L_{ijkl}(\boldsymbol{\xi})+\Gamma^L_{jikl}(\boldsymbol{\xi})+\Gamma^L_{ijlk}(\boldsymbol{\xi})+\Gamma^L_{jilk}(\boldsymbol{\xi})\right]g^2(\boldsymbol{\xi}),$$

$$P^\epsilon_{ij} = \frac{c}{1-c}\sum_{\substack{\mathrm{p}_n=-\infty\\ -\{\mathrm{p}_n=\mathrm{p}_s=0\}}}^{\infty}\sum_{\mathrm{p}_s=-\infty}^{\infty}\Gamma^e_{ij}(\boldsymbol{\xi})g^2(\boldsymbol{\xi}), \tag{40}$$

$$P^e_{ijk} = \frac{c}{1-c}\sum_{\substack{\mathrm{p}_n=-\infty\\ -\{\mathrm{p}_n=\mathrm{p}_s=0\}}}^{\infty}\sum_{\mathrm{p}_s=-\infty}^{\infty}\frac{1}{2}\left[\Gamma^e_{ijk}(\boldsymbol{\xi})+\Gamma^e_{jik}(\boldsymbol{\xi})\right]g^2(\boldsymbol{\xi})$$

$m \neq n \neq s$, where now $c = \pi a_n a_s/b_n b_s$,

$$\boldsymbol{\xi} = \mathrm{p}_n\mathbf{u}_n + \frac{b_n}{b_s}\mathrm{p}_s\mathbf{u}_s, \tag{41}$$

and

$$g(\xi) = \frac{J_1\left(2\pi\sqrt{\frac{a_n^2}{b_n^2}\mathrm{p}_n^2+\frac{a_s^2}{b_s^2}\mathrm{p}_s^2}\right)}{\pi\sqrt{\frac{a_n^2}{b_n^2}\mathrm{p}_n^2+\frac{a_s^2}{b_s^2}\mathrm{p}_s^2}} \tag{42}$$

with J_1 denoting the Bessel function of the first kind. Finally, the case of a *laminate* composite comprising alternating layers of piezoelectric materials $r = 1$ and $r = 2$ can be generated from expressions (37) by setting two of the semi-axes of the inclusion and the corresponding sides of the unit cell to be of infinite length. By setting $a_m,\ b_m = \infty$ and $a_n,\ b_n = \infty\,(m \neq n)$, for instance, the result reads as

$$P^L_{ijkl} = \frac{1}{4}\left[\Gamma^L_{ijkl}(\mathbf{u}_s)+\Gamma^L_{jikl}(\mathbf{u}_s)+\Gamma^L_{ijlk}(\mathbf{u}_s)+\Gamma^L_{jilk}(\mathbf{u}_s)\right],$$
$$P^\epsilon_{ij} = \Gamma^\epsilon_{ij}(\mathbf{u}_s),$$
$$P^e_{ijk} = \frac{1}{2}\left[\Gamma^e_{ijk}(\mathbf{u}_s)+\Gamma^e_{jik}(\mathbf{u}_s)\right] \tag{43}$$

$m \neq n \neq s$.

3.1.2. A periodic distribution of cuboidal inclusions

Next, we consider the same periodic distribution as in the preceding subsection but now the inclusions are taken to be of cuboidal shape. The unit cell here is also taken to be a rectangular prism of sides b_1, b_2, b_3 containing a single inclusion at its center, see Fig. 1(b). The sides of the inclusion are denoted by a_1, a_2, a_3 and its principal axes are aligned with the unit cell, and, therefore, also with the Cartesian laboratory axes $\mathbf{u}_1$, $\mathbf{u}_2$, $\mathbf{u}_3$. The microstructural tensors (31) in this case can be shown to reduce to expressions of the very form (37), where the vector ξ is still given by (38), but now the volume fraction $c = a_1a_2a_3/b_1b_2b_3$, and the function $g(\xi)$ is given in terms of the integers p_1, p_2, p_3 by

$$g(\xi) = \begin{cases} \dfrac{\sin\eta_1}{\eta_1}\dfrac{\sin\eta_2}{\eta_2}\dfrac{\sin\eta_3}{\eta_3} & \text{if} \quad \mathrm{p}_1,\mathrm{p}_2,\mathrm{p}_3 \neq 0 \\ \dfrac{\sin\eta_i}{\eta_i}\dfrac{\sin\eta_j}{\eta_j} & \text{if} \quad \mathrm{p}_i,\mathrm{p}_j \neq 0, \mathrm{p}_k = 0 \qquad i \neq j \neq k \\ \dfrac{\sin\eta_i}{\eta_i} & \text{if} \quad \mathrm{p}_i \neq 0, \mathrm{p}_j = \mathrm{p}_k = 0 \quad i \neq j \neq k \end{cases} \tag{44}$$

with

$$\eta_1 = \frac{a_1}{b_1}\pi\mathrm{p}_1, \quad \eta_2 = \frac{a_2}{b_2}\pi\mathrm{p}_2, \quad \eta_3 = \frac{a_3}{b_3}\pi\mathrm{p}_3, \tag{45}$$

instead of by (39).

The limiting case of a cuboidal distribution of *cubic inclusions* is generated by setting $a_1 = a_2 = a_3 = a$ in the above result. In turn, a rectangular distribution of aligned *cylindrical fibers* with rectangular cross section is generated by setting one of the semi-axes of the inclusion and the corresponding side of the unit cell to be unbounded. By setting a_m, $b_m = \infty$ as above, the microstructural tensors $\mathbf{P}^L$, $\mathbf{P}^\epsilon$, $\mathbf{P}^e$ reduce to expressions of the very form (40) with ξ given by (41), but now $c = a_n a_s/b_n b_s$ and

$$g(\xi) = \begin{cases} \dfrac{\sin\eta_n}{\eta_n}\dfrac{\sin\eta_s}{\eta_s} & \text{if} \quad \mathrm{p}_n,\mathrm{p}_s \neq 0 \\ \dfrac{\sin\eta_n}{\eta_n} & \text{if} \quad \mathrm{p}_s = 0 \\ \dfrac{\sin\eta_s}{\eta_s} & \text{if} \quad \mathrm{p}_n = 0 \end{cases} \tag{46}$$

with

$$\eta_n = \frac{a_n}{b_n}\pi\mathrm{p}_n, \quad \eta_s = \frac{a_s}{b_s}\pi\mathrm{p}_s, \tag{47}$$

$m \neq n \neq s$.

3.1.3. A random distribution of ellipsoidal inclusions

As a final example, we consider a random microstructure comprised of aligned homothetic ellipsoidal inclusions whose centers are distributed with the so-called "ellipsoidal" symmetry introduced by Willis (1977). The semi-axes of a typical inclusion are denoted by a_1, a_2, a_3 and, for convenience, its principal axes are aligned with the Cartesian laboratory axes $\mathbf{u}_1$, $\mathbf{u}_2$, $\mathbf{u}_3$; see Fig. 1(c). For this class of microstructures, the weighting function (19) can be determined explicitly allowing to write simple expressions for the microstructural tensors (31):

$$P^L_{ijkl} = \frac{a_2a_3}{16\pi a_1^2}\int_0^{2\pi}\int_{-1}^{1}\frac{\Gamma^L_{ijkl}(\xi)+\Gamma^L_{jikl}(\xi)+\Gamma^L_{ijlk}(\xi)+\Gamma^L_{jilk}(\xi)}{\left[(1-z^2)\left(\cos^2\theta+\frac{a_2^2}{a_1^2}\sin^2\theta\right)+\frac{a_3^2}{a_1^2}z^2\right]^{3/2}}\mathrm{d}z\mathrm{d}\theta,$$

$$P^\epsilon_{ij} = \frac{a_2a_3}{4\pi a_1^2}\int_0^{2\pi}\int_{-1}^{1}\frac{\Gamma^\epsilon_{ij}(\xi)}{\left[(1-z^2)\left(\cos^2\theta+\frac{a_2^2}{a_1^2}\sin^2\theta\right)+\frac{a_3^2}{a_1^2}z^2\right]^{3/2}}\mathrm{d}z\mathrm{d}\theta,$$

$$P^e_{ijk} = \frac{a_2a_3}{8\pi a_1^2}\int_0^{2\pi}\int_{-1}^{1}\frac{\Gamma^e_{ijk}(\xi)+\Gamma^e_{jik}(\xi)}{\left[(1-z^2)\left(\cos^2\theta+\frac{a_2^2}{a_1^2}\sin^2\theta\right)+\frac{a_3^2}{a_1^2}z^2\right]^{3/2}}\mathrm{d}z\mathrm{d}\theta, \tag{48}$$

where

$$\xi = \sqrt{1-z^2}\cos\theta\mathbf{u}_1 + \sqrt{1-z^2}\sin\theta\mathbf{u}_2 + z\mathbf{u}_3 \tag{49}$$

in terms of the integration variables z, θ.

The choice of semi-axes $a_1 = a_2 = a_3 = a$ in (48) corresponds to an isotropic distribution of *spherical inclusions*. Setting one of the semi-axes to be of infinite length corresponds in turn to the limiting case of aligned *cylindrical fibers* of elliptical cross section that are randomly distributed with "elliptical" symmetry in the transverse plane. Setting $a_m = \infty\,(m,\ n,\ s = 1,2,3)$, for instance, reduces expressions (48) to

$$P^L_{ijkl} = \frac{a_s}{8\pi a_n}\int_0^{2\pi}\frac{\Gamma^L_{ijkl}(\xi)+\Gamma^L_{jikl}(\xi)+\Gamma^L_{ijlk}(\xi)+\Gamma^L_{jilk}(\xi)}{\cos^2\theta+\frac{a_s^2}{a_n^2}\sin^2\theta}\mathrm{d}\theta,$$

$$P^\epsilon_{ij} = \frac{a_s}{2\pi a_n}\int_0^{2\pi}\frac{\Gamma^\epsilon_{ij}(\xi)}{\cos^2\theta+\frac{a_s^2}{a_n^2}\sin^2\theta}\mathrm{d}\theta,$$

$$P^e_{ijk} = \frac{a_s}{4\pi a_n}\int_0^{2\pi}\frac{\Gamma^e_{ijk}(\xi)+\Gamma^e_{jik}(\xi)}{\cos^2\theta+\frac{a_s^2}{a_n^2}\sin^2\theta}\mathrm{d}\theta \tag{50}$$

$m \neq n \neq s$, where now

$$\xi = \cos\theta\mathbf{u}_n + \sin\theta\mathbf{u}_s. \tag{51}$$

Setting two of the semi-axes in (48) to be unbounded corresponds in turn to the limiting case of a *laminate* composite where layers of piezoelectric materials $r = 1$ and $r = 2$ are randomly

Table 1
Density (ρ [kg/m^3]), and elastic (L_{ijkl} [GPa]), dielectric (ϵ_{ij} [nC/Vm]), and piezoelectric (e_{ijk} [C/m^2]) components for the constituent materials used for the sample results.

	PZT-7A	PZT–PNN	Mn-doped PZT	Barium Sodium Niobate	Araldite D	Air
ρ	7600	7500	5700	5300	1150	1.225
L_{1111}	148	127.2	148	238.9	8	0.0
L_{2222}	148	127.2	148	247.4	8	0.0
L_{3333}	111	117.4	131	135.1	8	0.0
L_{1122}	76.3	80.21	76.2	104.2	4.4	0.0
L_{1133}	74.3	84.67	74.2	50.06	4.4	0.0
L_{2233}	74.3	84.67	74.2	52.14	4.4	0.0
L_{1212}	35.85	23.47	35.9	75.76	1.8	0.0
L_{1313}	25.3	22.99	25.4	65.79	1.8	0.0
L_{2323}	25.3	22.99	25.4	64.94	1.8	0.0
ϵ_{11}	4.11525	27.71	7.965	2.081	0.0354	0.00885
ϵ_{22}	4.11525	27.71	7.965	2.187	0.0354	0.00885
ϵ_{33}	2.09745	30.1	8.38502	0.4516	0.0354	0.00885
e_{113}	9.2	17	11.4	2.763	0.0	0.0
e_{223}	9.2	17	11.4	3.377	0.0	0.0
e_{311}	−2.3	−6.62	−4.3	−0.445	0.0	0.0
e_{322}	−2.3	−6.62	−4.3	−0.285	0.0	0.0
e_{333}	9.3	23.2	12.5	4.335	0.0	0.0

Table 2
Relations among the various types of elastic, dielectric, and piezoelectric moduli.

$\tilde{L}_{ijpq}\tilde{M}_{pqkl} = \frac{1}{2}(\delta_{ik}\delta_{jl}+\delta_{il}\delta_{jk})$
$\tilde{L}^{\mathbf{D}}_{ijpq}\tilde{M}^{\mathbf{D}}_{pqkl} = \frac{1}{2}(\delta_{ik}\delta_{jl}+\delta_{il}\delta_{jk})$
$\tilde{\epsilon}_{ik}\tilde{B}_{kj} = \delta_{ij}$
$\tilde{\epsilon}^{\mathbf{S}}_{ik}\tilde{B}^{\mathbf{S}}_{kj} = \delta_{ij}$
$\tilde{d}_{nkl} = \tilde{\epsilon}^{\mathbf{S}}_{nm}\tilde{g}_{mkl} = \tilde{e}_{nij}\tilde{M}_{ijkl}$
$\tilde{e}_{nkl} = \tilde{\epsilon}_{nm}\tilde{h}_{mkl} = \tilde{d}_{nij}\tilde{L}_{ijkl}$
$\tilde{g}_{nkl} = \tilde{B}^{\mathbf{S}}_{nm}\tilde{d}_{mkl} = \tilde{h}_{nij}\tilde{M}^{\mathbf{D}}_{ijkl}$
$\tilde{h}_{nkl} = \tilde{B}_{nm}\tilde{e}_{mkl} = \tilde{g}_{nij}\tilde{L}^{\mathbf{D}}_{ijkl}$
$\tilde{L}^{\mathbf{D}}_{ijkl} - \tilde{L}_{ijkl} = \tilde{e}_{mij}\tilde{h}_{mkl}$
$\tilde{M}_{ijkl} - \tilde{M}^{\mathbf{D}}_{ijkl} = \tilde{d}_{mij}\tilde{g}_{mkl}$
$\tilde{\epsilon}^{\mathbf{S}}_{mn} - \tilde{\epsilon}_{mn} = \tilde{d}_{nkl}\tilde{e}_{mkl}$
$\tilde{B}_{mn} - \tilde{B}^{\mathbf{S}}_{mn} = \tilde{h}_{nkl}\tilde{g}_{mkl}$

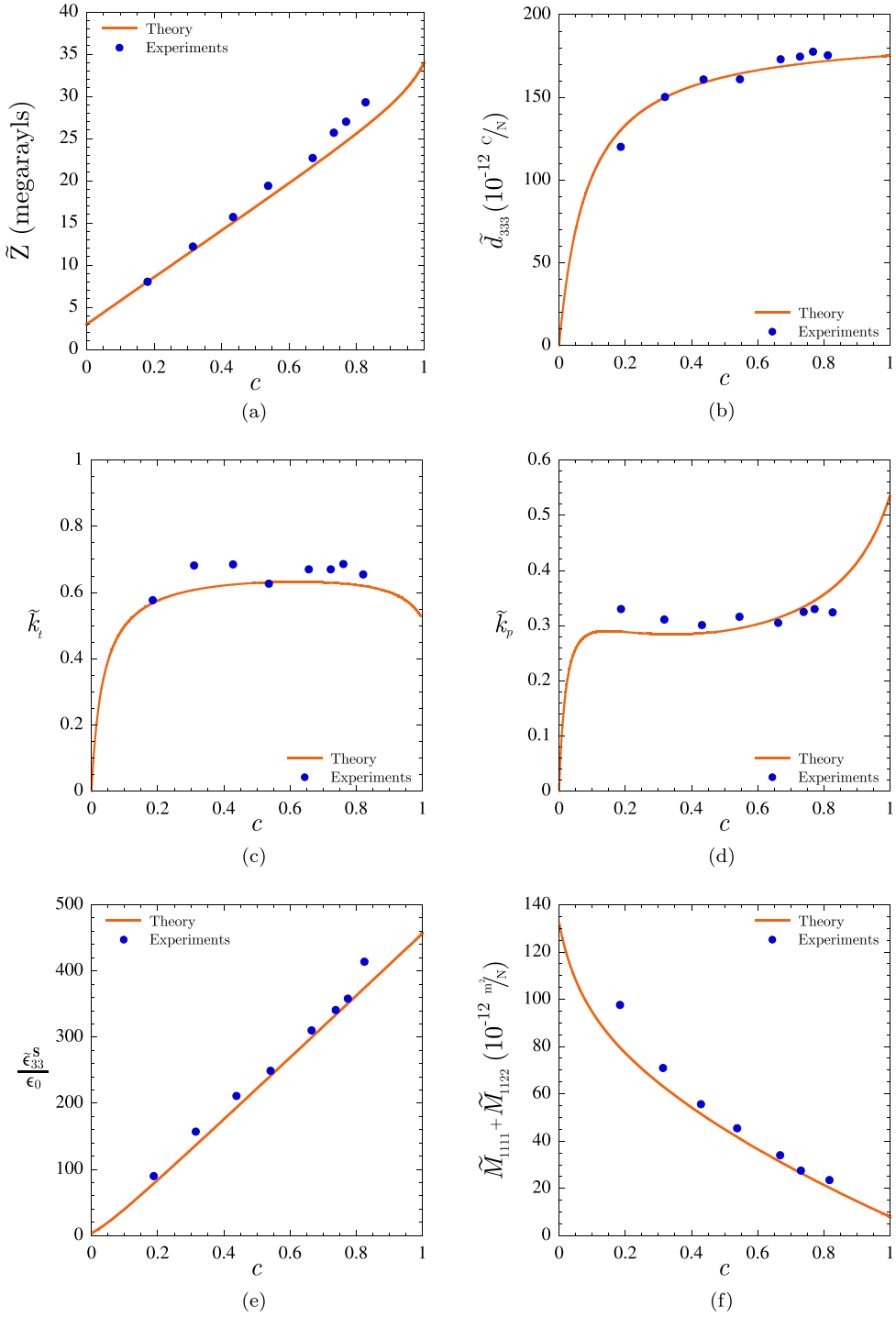

Fig. 2. The theoretical solution (36) compared to the experimental results of Chan and Unsworth (1989) for the overall response of an Araldite D matrix reinforced by PZT-7A cylindrical fibers. Results are shown for: (a) the specific acoustic impedance $\tilde{Z}$, (b) the piezoelectric component $\tilde{d}_{333}$, (c) the thickness electromechanical coupling factor $\tilde{k}_t$, (d) the planar electromechanical coupling factor $\tilde{k}_p$, (e) the "free" dielectric component $\tilde{\epsilon}^{\mathbf{S}}_{33}/\epsilon_0$, and (f) the compliance $\tilde{M}_{1111}+\tilde{M}_{1122}$, all as functions of the volume fraction of fibers c.

alternated. Setting $a_m = \infty$ and $a_n = \infty$ $(m \neq n)$ as in the foregoing, reduces the microstructural tensors (48) to the same expressions (43) obtained for the laminate composite with periodically alternating layers of materials $r = 1$ and $r = 2$.

4. Sample results

In the sequel, we confront the theoretical solution (36) to five different sets of experimental data and full-field simulations available in the literature. The first set of results pertains to a fiber-reinforced composite made up of a single family of aligned cylindrical PZT-7A fibers of circular cross section embedded in a polymeric matrix. The second set pertains to a PZT–PNN matrix weakened by a periodic array of aligned cylindrical pores of elliptical cross section. The third set corresponds to a hot-pressed Mn-doped PZT material containing a random distribution of aligned spheroidal pores. Finally, the fourth and fifth sets of results correspond to a barium sodium niobate matrix weakened by periodic

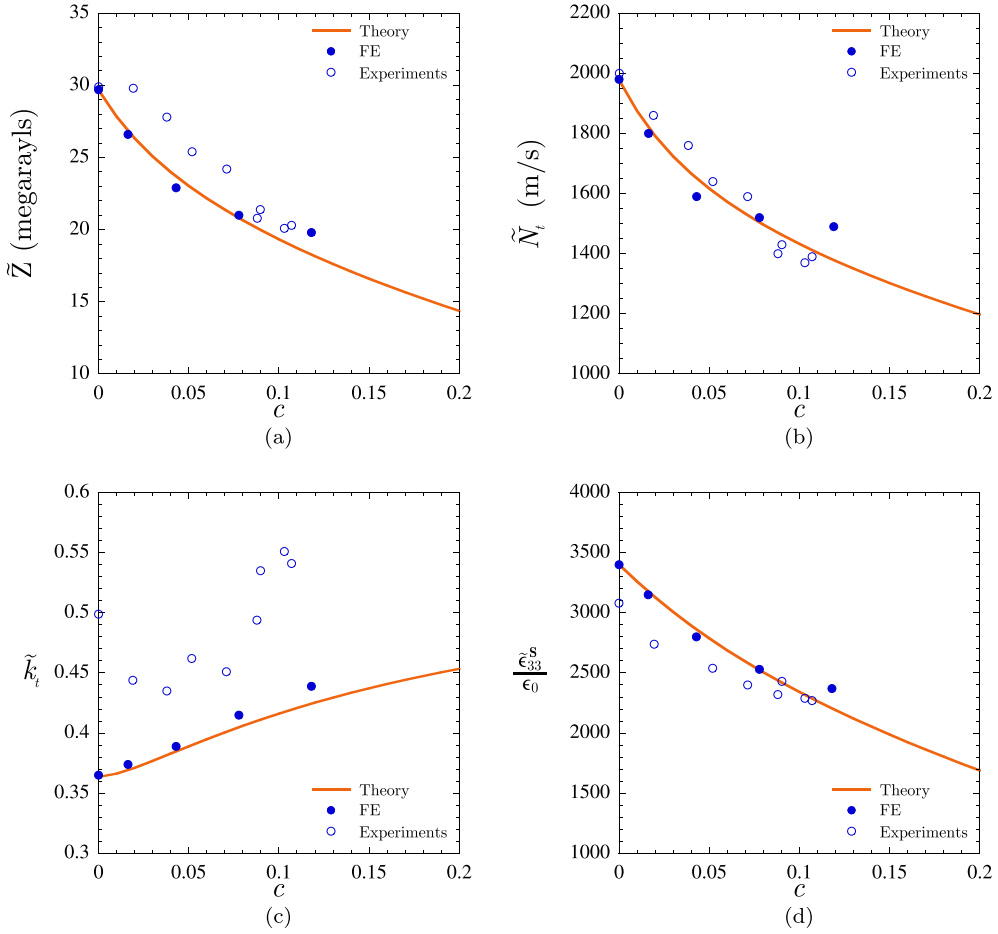

Fig. 3. The theoretical solution (36) compared to the experimental results of Bast and Wersing (1989) and the finite element simulations (FE) of Kar-Gupta and Venkatesh (2006) for the overall response of a PZT–PNN matrix containing a periodic rectangular distribution of aligned cylindrical pores with elliptical cross-section. Results are shown for: (a) the specific acoustic impedance $\tilde{Z}$, (b) the frequency constant $\tilde{N}_t$, (c) the thickness electromechanical coupling factor $\tilde{k}_t$, and (d) the "free" dielectric component $\tilde{\epsilon}^{\mathbf{S}}_{33}/\epsilon_0$, all as functions of the volume fraction of pores c.

distributions of spherical and cuboidal pores. This broad range of comparisons aim at illustrating not only the descriptive and predictive capabilities of the result (36), but also its potential deployment as a bottom-up material design tool.

Before proceeding with the presentation of the results, it is expedient to record the properties of the various underlying (matrix and inclusion) constituents and macroscopic quantities that are involved in the comparisons. Table 1 provides the material properties of the constituents in component form; following standard practice, the Cartesian laboratory axes $\mathbf{u}_3$ is chosen to indicate the poling direction throughout this section.

Table 2 provides the relations between the effective "short-circuit" elasticity tensor $\tilde{\mathbf{L}}$, effective "clamped" dielectric tensor $\tilde{\boldsymbol{\epsilon}}$, and effective piezoelectric tensor $\tilde{\mathbf{e}}$ given by (36) with the alternative effective tensors: $\tilde{\mathbf{L}}^{\mathbf{D}}$ is the "open-circuit" (measured at constant electric displacement) elasticity tensor; $\tilde{\mathbf{M}}$ and $\tilde{\mathbf{M}}^{\mathbf{D}}$ are the "short-circuit" and "open-circuit" compliance tensors; $\tilde{\boldsymbol{\epsilon}}^{\mathbf{S}}$ is the "free" (measured at constant stress) dielectric tensor; $\tilde{\mathbf{B}}$ and $\tilde{\mathbf{B}}^{\mathbf{S}}$ are the "clamped" and "free" impermeability tensors; $\tilde{\mathbf{d}}$, $\tilde{\mathbf{g}}$, and $\tilde{\mathbf{h}}$ are the alternative piezoelectric tensors (see, e.g., Standards on Piezoelectric Crystals, 1949). Once $\tilde{\mathbf{L}}$, $\tilde{\boldsymbol{\epsilon}}$, and $\tilde{\mathbf{e}}$ are generated from (36), any of the components of these alternative effective tensors can be readily computed. Of particular interest here are the specific acoustic impedance $\tilde{Z}$ and frequency constant $\tilde{N}_t$ defined by

$$\tilde{Z} = \sqrt{\bar{\rho}\tilde{L}^{\mathbf{D}}_{3333}} \quad \text{and} \quad \tilde{N}_t = \frac{1}{2}\sqrt{\frac{\tilde{L}_{3333}}{\bar{\rho}}} \tag{52}$$

with $\bar{\rho} = (1-c)\rho^{(1)} + c\rho^{(2)}$ denoting the average density of the composite, the hydrostatic coefficients $\tilde{d}_h$ and $\tilde{g}_h$ given by

$$\tilde{d}_h = \tilde{d}_{311} + \tilde{d}_{322} + \tilde{d}_{333} \quad \text{and} \quad \tilde{g}_h = \tilde{g}_{311} + \tilde{g}_{322} + \tilde{g}_{333}, \tag{53}$$

and the thickness and planar electromechanical coupling factors $\tilde{k}_t$ and $\tilde{k}_p$ defined by

$$\tilde{k}_t = \sqrt{1 - \frac{\tilde{L}_{3333}}{\tilde{L}^{\mathbf{D}}_{3333}}} \quad \text{and} \quad \tilde{k}_p = \sqrt{1 - \frac{\tilde{\epsilon}_{33}\tilde{L}^{\mathbf{D}}_{3333}}{\tilde{\epsilon}^{\mathbf{S}}_{33}\tilde{L}_{3333}}}. \tag{54}$$

4.1. A fiber-reinforced composite with polymeric matrix and piezoelectric fibers

We begin by confronting the theoretical solution (36) to the experimental measurements of Chan and Unsworth (1989) for the overall response of piezoelectric composites made up of a single family of PZT-7A cylindrical fibers, with the poling direction $\mathbf{u}_3$ aligned with the direction of the fibers, embedded in an Araldite D matrix. The properties of the PZT-7A and Araldite D materials are given in Table 1. Chan and Unsworth did report that their specimens were fabricated by means of a dice-and-fill technique — which allowed them to reach volume fractions of fibers up to $c = 0.82$ — but did not provide details about the cross-sectional shape nor spatial distribution of the fibers. Here, we assume that the fibers have circular cross section and that they are isotropically distributed in the transverse plane. The appropriate microstructrual

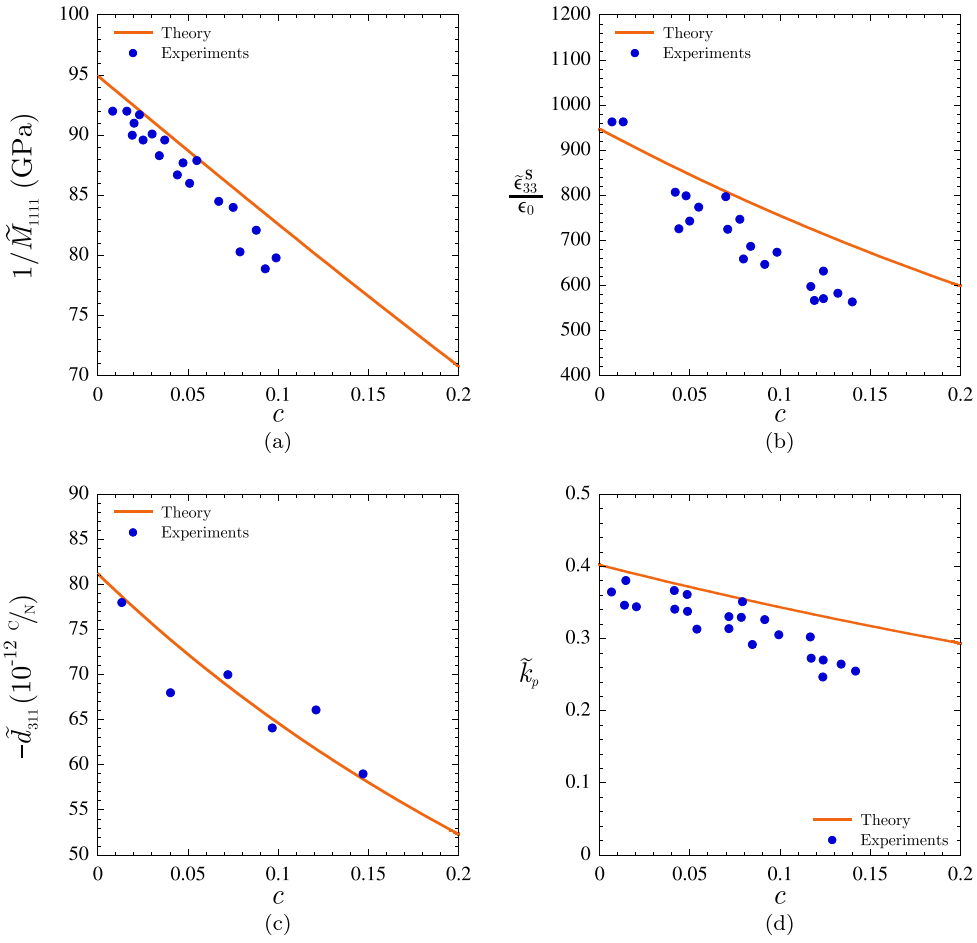

Fig. 4. The theoretical solution (36) compared to experimental results (Banno, 1987) for the overall response of a hot-pressed Mn-doped PZT material containing a random distribution of aligned oblate spheroidal pores. Results are shown for: (a) the elastic constant $1/\tilde{M}_{1111}$, (b) the "free" dielectric component $\tilde{\epsilon}^{\mathbf{S}}_{33}/\epsilon_0$, (c) the piezoelectric component $-\tilde{d}_{311}$, and (d) the planar electromechanical coupling factor $\tilde{k}_p$, all as functions of the volume fraction of pores c.

tensors $\mathbf{P}^L$, $\mathbf{P}^\epsilon$, $\mathbf{P}^e$ within the context of the solution (36) are thus given by expressions (50) with $m = 3$, $n = 2$, $s = 1$, and $a_1 = a_2 = a$.

Fig. 2 shows results for the following overall properties of the composite: (a) the specific acoustic impedance $\tilde{Z}$, (b) the piezoelectric component $\tilde{d}_{333}$, (c) the thickness electromechanical coupling factor $\tilde{k}_t$, (d) the planar electromechanical coupling factor $\tilde{k}_p$, (d) the "free" dielectric component $\tilde{\epsilon}^{\mathbf{S}}_{33}/\epsilon_0$, and (f) the compliance $\tilde{M}_{1111} + \tilde{M}_{1122}$, all as functions of the volume fraction of the PZT-7A fibers c. It is plain from this figure that the predictions from the theoretical solution (36), the solid lines in the plots, are consistently in good agreement with the experimental measurements of Chan and Unsworth (1989), the solid circles.

4.2. A porous piezoelectric composite with cylindrical pores

Next, we compare the predictions of the theoretical solution (36) with the experimental results of Bast and Wersing (1989) for the overall response of a PZT–PNN matrix containing a rectangular array of aligned cylindrical pores transverse to the poling direction $\mathbf{u}_3$. Unfortunately, Bast and Wersing did not report all of the material properties of the type of PZT–PNN utilized in their experiments. We assume that they are given by those recorded in Table 1, while the pores are taken to be filled by air at atmospheric pressure. On the other hand, Bast and Wersing (1989) did provide SEM images of their specimens from which information about the size, shape, and spatial distribution of the pores can be estimated. Based on these images, the fibers are known to be aligned with the $\mathbf{u}_2$ direction, their cross sections are taken to be elliptical with an aspect ratio of $17/75 \approx 0.23$, and the unit cell describing their periodic rectangular distribution is taken to have an aspect ratio of $76/215 \approx 0.35$. The corresponding microstructural tensors $\mathbf{P}^L$, $\mathbf{P}^\epsilon$, $\mathbf{P}^e$ required in the computation of (36) are thus given by expressions (40) with $m = 2$, $n = 1$, $s = 3$, $a_3/a_1 = 17/75 \approx 0.23$, and $b_3/b_1 = 76/215 \approx 0.35$.

Fig. 3 shows results for: (a) the specific acoustic impedance $\tilde{Z}$, (b) the frequency constant $\tilde{N}_t$, (c) the thickness electromechanical coupling factor $\tilde{k}_t$, and (d) the "free" dielectric component $\tilde{\epsilon}^{\mathbf{S}}_{33}/\epsilon_0$, all as functions of the volume fraction of pores c. The solid lines correspond to the predictions from the theoretical solution (36), while the hollow circles correspond to the experimental results of Bast and Wersing (1989). The finite element (FE) simulations of the Bast and Wersing experiments by Kar-Gupta and Venkatesh (2006) are also included in the plots (solid circles) for further scrutiny of the theoretical predictions. All three sets of results are seen to be in reasonably good agreement.

4.3. A porous piezoelectric composite with a random distribution of aligned spheroidal pores

In this subsection, we compare the theoretical predictions generated from (36) with the experimental data of Okazaki et al. reported by Banno (1987) for the overall response of Mn-doped PZT ceramics containing a random distribution of spheroidal pores aligned with the poling direction $\mathbf{u}_3$. As a complete set of material parameters for the Mn-doped PZT utilized by these authors was not provided, we use the approximate values reported in Table 1. The pores are assumed to be vacuous. In his paper, Banno (1987)

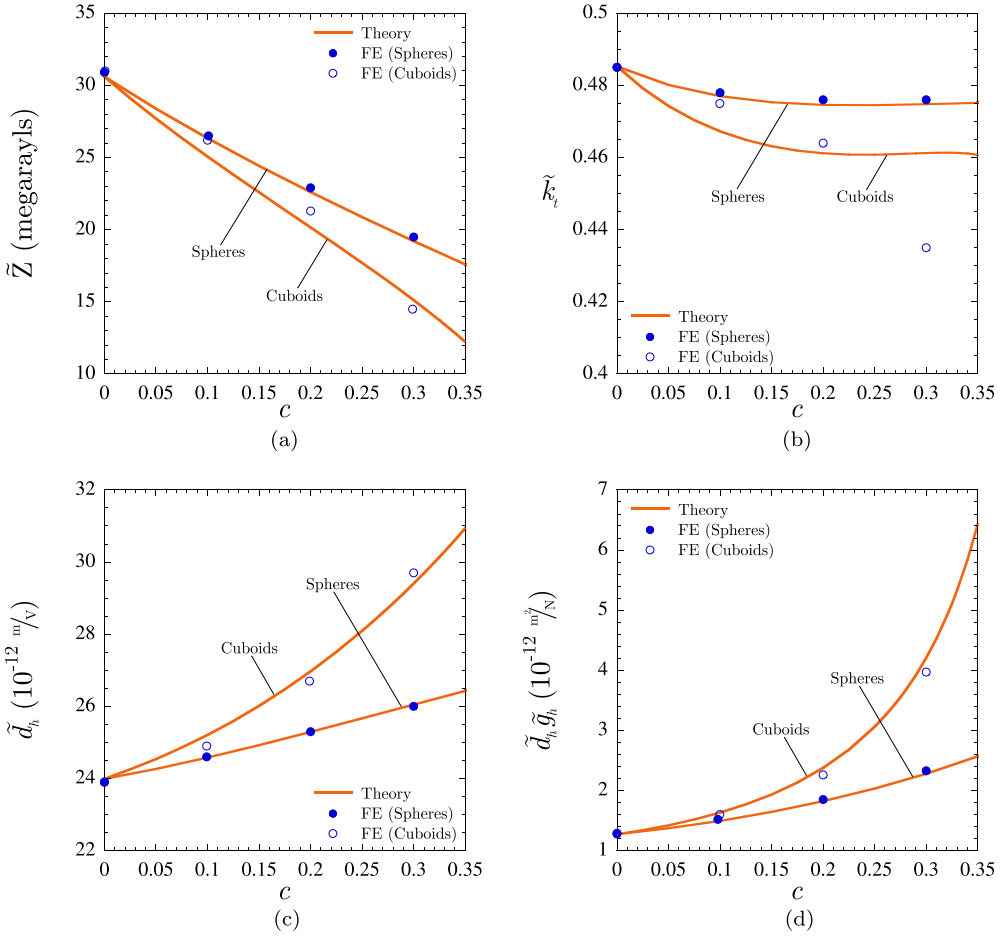

Fig. 5. The theoretical solution (36) compared to the full-field simulations of Sumantu and Venkatesh (2011) for the overall response of a barium sodium niobate matrix containing a periodic cubic distribution of spherical and cuboidal pores. Results are shown for (a) the specific acoustic impedance $\tilde{Z}$, (b) the thickness electromechanical coupling factor $\tilde{k}_t$, (c) the hydrostatic piezoelectric coefficient $\tilde{d}_h$, and (d) the hydrostatic constant $\tilde{d}_h\tilde{g}_h$ as functions of the volume fraction of pores c.

did include SEM images of the underlying pores, from which one can deduce that they are approximately oblate spheroids with an aspect ratio of $1/3 \approx 0.33$ and that their small semi-axis is aligned in the poling direction $\mathbf{u}_3$. No information was reported regarding the spatial distribution of the pores. However, given that the specimens were fabricated by means of a hot pressing technique, it is reasonable to approximate their spatial distribution as being "spheroidal" in the sense of Willis (1977), as opposed to merely isotropic. In view of this microstructural information, the appropriate tensors $\mathbf{P}^L$, $\mathbf{P}^\epsilon$, $\mathbf{P}^e$ required in the computation of (36) are given by expressions (48) with $a_2/a_1 = 1$ and $a_3/a_1 = 1/3 \approx 0.33$.

Fig. 4 shows results for: (a) the elastic constant $1/\tilde{M}_{1111}$, (b) the "free" dielectric component $\tilde{\epsilon}^{\mathbf{S}}_{33}/\epsilon_0$, (c) the piezoelectric component $-\tilde{d}_{311}$, and (d) the planar electromechanical coupling factor $\tilde{k}_p$ in terms of the volume fraction of pores c. Consistent with the two previous sets of results, all of the theoretical predictions (solid lines) are seen to be in good agreement with the experimental measurements (solid circles) reported by Banno (1987).

4.4. Porous piezoelectric composites with periodic distributions of spherical and cuboidal pores

Finally, the theoretical solution (36) is confronted to the full-field simulations of Sumantu and Venkatesh (2011) for the overall response of a barium sodium niobate matrix weakened by a periodic cubic distribution of spherical and cuboidal vacuous pores. The properties of the barium sodium niobate material utilized in the simulations are provided in Table 1. Based on an image reported by these authors, the cuboidal pores are taken here to be of square cross section, to have an aspect ratio of 0.45, and to have their smallest side aligned with the poling direction $\mathbf{u}_3$. For the microstructure with spherical pores, the tensors $\mathbf{P}^L$, $\mathbf{P}^\epsilon$, $\mathbf{P}^e$ required in the computation of (36) are given by expressions (37) with sides of the unit cell $b_1 = b_2 = b_3 = b$ and the function $g(\xi)$ given by (39) with $a_1 = a_2 = a_3 = a$. For the microstructure with cuboidal pores, the tensors $\mathbf{P}^L$, $\mathbf{P}^\epsilon$, $\mathbf{P}^e$ are also given by expressions (37) with $b_1 = b_2 = b_3 = b$, but now the function $g(\xi)$ is given by (44) with $a_1 = a_2$ and $a_3/a_1 = 0.45$.

Fig. 5 shows results for: (a) the specific acoustic impedance $\tilde{Z}$, (b) the thickness electromechanical coupling factor $\tilde{k}_t$, (c) the hydrostatic piezoelectric coefficient $\tilde{d}_h$, and (d) the hydrostatic constant $\tilde{d}_h\tilde{g}_h$, all as functions of the volume fraction of pores. The solid lines correspond to the predictions from the theoretical solution (36), while the solid and hollow circles correspond to the simulations of Sumantu and Venkatesh (2011) for the composites with spherical and cuboidal pores, respectively. Save for the $\tilde{k}_t$ results shown in Fig. 5(b) for the microstructure with cuboidal pores, all of the theoretical predictions are seen to be in good agreement with the full-field simulations.

In short, the above sample results have illustrated the far-reaching capabilities of the theoretical result (36) to describe and predict the behavior of large classes of piezoelectric composites with particulate microstructures. In view of its microscopic nature, generality, and analytical tractability, the result (36) provides thus a

robust tool to efficiently guide the design of piezoelectric composites with desired macroscopic properties from the bottom up. Such material design problems are worth pursuing in future works.

Acknowledgment

Support for this work by the National Science Foundation through CAREER Grant CMMI–1219336 is gratefully acknowledged.

References

Banno, H., 1987. Effects of shape and volume fraction of closed pores on dielectric, elastic, and electromechanical properties of dielectric and piezoelectric ceramics — a theoretical approach. Am. Ceram. Soc. Bull. 66, 1332–1337.

Bast, U., Wersing, W., 1989. The influence of internal voids with 3–1 connectivity on the properties of piezoelectric ceramics prepared by a new planar process. Ferroelectrics 94, 229–242.

Bisegna, P., Luciano, R., 1996. Variational bounds for the overall properties of piezoelectric composites. J. Mech. Phys. Solids 44, 583–602.

Chan, H.L.W., Unsworth, J., 1989. Simple model for piezoelectric ceramic/polymer 1–3 composites used in ultrasonic transducer applications. IEEE Trans. Ultrason. Ferroelectr. Freq. Control 36, 434–441.

Deeg, W.F., 1980. The Analysis of Dislocation, Crack, and Inclusion Problems in Piezoelectric Solids, Ph.D. dissertation. Stanford University, USA.

Dorfmann, A., Ogden, R.W., 2005. Nonlinear electroelasticity. Acta Mech. 174, 167–183.

Dunn, M.L., Taya, M., 1993. An analysis of piezoelectric composite materials containing ellipsoidal inhomogeneities. Proc. R. Soc. Lond. A 443, 265–287.

Kar-Gupta, R., Venkatesh, T.A., 2006. Electromechanical response of porous piezoelectric materials. Acta Mater. 54, 4063–4078.

Kittel, C., 2005. Introduction to Solid State Physics. John Wiley & Sons Inc., New York.

Li, J.Y., Dunn, M., 2001. Variational bounds for the effective moduli of heterogeneous piezoelectric solids. Philos. Mag. A 81, 903–926.

Lopez-Pamies, O., 2014. Elastic dielectric composites: theory and application to particle-filled ideal dielectrics. J. Mech. Phys. Solids 64, 61–82.

Milton, G.W., 2002. The Theory of Composites. Cambridge Monographs on Applied and Computational Mathematics, vol. 6. Cambridge University Press, Cambridge.

Olson, T., Avellaneda, M., 1992. Effective dielectric and elastic constants of piezoelectric polycrystals. J. Appl. Phys. 71, 4455–4464.

Standards on Piezoelectric Crystals, 1949. Proc. I.R.E. 37, pp. 1378–1395.

Sumantu, I., Venkatesh, T.A., 2011. Electromechanical response of (3–0) porous piezoelectric materials: effects of porosity shape. J. Appl. Phys. 110, 034109.

Suo, Z., Zhao, X., Greene, W.H., 2008. A nonlinear field theory of deformable dielectrics. J. Mech. Phys. Solids 56, 467–486.

Willis, J.R., 1977. Bounds and self-consistent estimates for the overall moduli of anisotropic composites. J. Mech. Phys. Solids 25, 185–202.